frontiers in Materials

REVIEW
published: 05 August 2020
doi: 10.3389/fmats.2020.00206

Recent Developments of Mn(II)-Doped 2D-Layered and 2D Platelet Perovskite Nanostructures

Samrat Das Adhikari and Narayan Pradhan**

School of Materials Sciences, Indian Association for the Cultivation of Science, Kolkata, India

Two-dimensional (2D) layered perovskites recently emerged as one of the most promising materials for optoelectronics. These not only behave like a quantum well structures, but also on doping Mn(II) ions at the Pb site result as a highly emissive doped material. These structures can also be used as a starting material for obtaining 3D perovskites. Thermal treatment of Mn(II)-incorporated layered perovskites in presence of Cs(I) ions led to Mn(II)-doped 2D platelet–shaped perovskites, which also tune their dimensions with varying dopant ion concentrations. Keeping the importance of the 2D-layered perovskites, this review focused on the basic structures to the recently developed synthetic strategies and their optical properties of layered structured perovskites, Mn(II)-doped layered perovskites, and Mn(II)-doped 2D platelet–shaped perovskites.

Keywords: lead halide perovskite, Ruddlesden–Popper perovskites, Mn doping, structure of layered perovskites, $CsPbCl_3$ 2D nanoplatelets

OPEN ACCESS

Edited by:
Jiatao Zhang,
Beijing Institute of Technology, China

Reviewed by:
Way Foong Lim,
Universiti Sains Malaysia (USM), Malaysia
Hongbo Li,
Beijing Institute of Technology, China

****Correspondence:***
Samrat Das Adhikari
sda.chemist@gmail.com
Narayan Pradhan
camnp@iacs.res.in

Specialty section:
This article was submitted to Colloidal Materials and Interfaces, a section of the journal Frontiers in Materials

Received: *19 November 2019*
Accepted: *05 June 2020*
Published: *05 August 2020*

Citation:
Das Adhikari S and Pradhan N (2020) Recent Developments of Mn(II)-Doped 2D-Layered and 2D Platelet Perovskite Nanostructures. Front. Mater. 7:206. doi: 10.3389/fmats.2020.00206

INTRODUCTION

Lead halide perovskite nanostructures recently emerged as the most promising materials for photovoltaic and optoelectronic applications (Kojima et al., 2009; Kovalenko et al., 2017; Jena et al., 2019; Li and Yang, 2019; Smith et al., 2019), which possess very high absorption coefficient, can achieve near unity photoluminescence quantum efficiency in different colors, and also can be efficiently doped for enhancing carrier transportation ability (Snaith, 2013; Kim et al., 2016; Di Stasio et al., 2017; Yong et al., 2018; Das Adhikari et al., 2019b; Dutta A. et al., 2019; Mondal et al., 2019; Park et al., 2019; Zhang et al., 2019). Significant achievements have been obtained in designing different all-inorganic and hybrid nanostructures, and their photophysical properties were also largely studied. Among these, two-dimensional (2D) layered perovskites and also 2D platelets of all inorganic perovskites remained promising for obtaining films with efficient activity and also confining the exciton within a limited boundary (Li et al., 2018; Mauck and Tisdale, 2019). Before discussing more on these 2D perovskites, details of the compositions and their possible structural variations are briefly discussed.

Lead halide perovskite is typically known in the formula $APbX_3$, where 'A' is a monovalent cation (Cs^+/Rb^+/methylammonium, formadinium, etc.), and 'X' is the halide ions. Generally, $APbX_3$ absorbs and emits visible light and is highly tunable with the composition of halide ions. In a report by Kovalenko et al., the emission of $FAPbI_3$ is further red tuned to the NIR region (780 nm) (Protesescu et al., 2017). These 'A' cations are placed at the octahedral cavity of eight corner-shared $[PbX_6]^{4-}$ octahedra moiety (Nedelcu et al., 2015; Protesescu et al., 2015; Leijtens et al., 2017; Beck et al., 2019). Varying 'A' cations in $APbX_3$ typically retain their physical properties, irrespective to their nature, either inorganic Cs^+ or organic methylammonium or formadinium ions

(Protesescu et al., 2016; Chen et al., 2018; Kanwat et al., 2018; Kato et al., 2018). But, in case of hybrid organic–inorganic–based perovskites, when the chain length of the 'A' cation becomes too large to fit within the octahedral cavity, each layer of the corner shared $[PbX_6]^{4-}$ separates and conjugated by two flipped large organic ammonium cations, which are mentioned as "spacer ligands" and form Ruddlesden–Popper phase perovskite, simply known as layered perovskite. The spacer ligands are basically large organic ammonium cations (RNH_3^+), and the halides are bonded through hydrogen bonding with the ammonium ion (Smith et al., 2014; Dou et al., 2015; Kumar et al., 2016; Mao et al., 2016; Pedesseau et al., 2016; Weidman et al., 2016; Lermer et al., 2018; Sheikh et al., 2018; Yin et al., 2018). Because the spacer ligands are insulating, these structures behave as multiple quantum wells. In this case, the inorganic layers act as the wells, where the spacer ligands serve as the potential barriers (Lan et al., 2019; Sichert et al., 2019; Soe et al., 2019).

Apart from the 3D $APbX_3$ perovskites, recent reports are strongly focused on these 2D-layered perovskites because of their high degree of structural flexibility and tunable optoelectronic properties (Even et al., 2014; Pedesseau et al., 2016; Stoumpos et al., 2016a,b; Tsai et al., 2016; Blancon et al., 2017). The optical bandgap of these layered perovskites is highly tunable by exchanging the halides accordingly (Weidman et al., 2016; Smith et al., 2017). Apart from this, a recent report also depicts the optical bandgap tunability as a function of chain length of the spacer ligand, where the blue shift with increasing the chain length is observed because of the change in octahedral tilting (Sichert et al., 2019). So, the synthetic development of these layered perovskites is necessary, which can prepare a set of visible light absorbing and emitting 2D-layered perovskites (Koutselas et al., 2011; Liang et al., 2016; Vassilakopoulou et al., 2016; Yuan et al., 2016; Cortecchia et al., 2017; Sun et al., 2019). Mn doping in these 2D-layered perovskite nanocrystals facilitate a dual emission window, one is from the host nanocrystal, and the secondary emission is from the Mn(II) dopant, which possess very high quantum yield, and to date reported as 97%, to the best of our knowledge (Biswas et al., 2017; Ba et al., 2019; Bakthavatsalam et al., 2019; Dutta S. K. et al., 2019; Luo et al., 2019; Sheikh and Nag, 2019; Sun et al., 2019). The optical emission generated from the dopant state is highly dependent on the dopant concentration. Apart from this, the doped layered perovskites are also used as the template for the preparation of 3D-doped perovskite nanocrystals, by the thermal treatment of layered perovskite and Cs^+ precursor (Das Adhikari et al., 2018; Parobek et al., 2018). Keeping all these issues in mind, this review focuses on the recent synthetic development and the structural and optical properties of these doped and undoped layered perovskites and also their use as a template for the preparation of 2D platelet perovskites.

STRUCTURE OF 2D-LAYERED PEROVSKITES

The general structural formula of Ruddlesden–Popper phase perovskite is $L_2(APbX_3)_{n-1}Pb_nX_4$. The integer, n, is the number of corner-shared $[PbX_6]^{4-}$ layers, separated by the two large organic ammonium ions. The simplest structure of this kind of perovskite is L_2PbX_4, when the value of n is 1 (Weidman et al., 2016). **Figure 1A** shows the typical structure of corner-shared octahedra separate by the spacer ligands (L), and form the layered perovskite, L_2PbX_4. The transmission electron microscopic (TEM) images are presented in **Figures 1B,C** for L_2PbCl_4 and L_2PbBr_4, respectively. The lateral dimension of these layered structures is generally several hundred nanometers to micron. This highly oriented stacked layered structure has a repetitive powder x-ray diffraction (XRD) pattern at (00n) peaks. From this XRD pattern, the distance between two successive layers can be calculated from the difference in diffraction angle of two repetitive (00n) peaks. **Figure 1D** represents such XRD patterns of three different-layered structures composed of butylammonium (BA), octylammonium (OA), and their equimolar mixture as the spacer ligand (L). In this case, the OA ligands occupy 2.1-nm distances between two inorganic layers, whereas BA ligands occupy 1.3-nm distances, which has a good agreement with their corresponding chain lengths.

The layered perovskite, L_2PbX_4, has halide ions–dependent bandgap tunability, which is a well-known fact for their 3D counterpart ($APbX_3$). The anion exchange in layered perovskites, L_2PbX_4, is first reported by Weidman et al. (2016), by mixing the pure L_2PbX_4 with 10% proportion and controlled further to study the successive red shift of bandgap energy going from chloride to iodide. **Figure 1E** shows a set of absorption spectra of pure and mixed halide-based layered perovskite. The absorption band edge shifts at the lower wavelength, when the Cl^- ions were replaced by Br^- and followed by I^- ions from partially to completely. L_2PbCl_4 has the absorption band edge near 334 nm (∼3.7 eV), which shows no optical emission because of its very high bandgap. L_2PbBr_4 has an absorption band edge near 400 nm, which has similar optical properties to 3D $CsPbCl_3$. For this reason, Mn^{2+} doping is found to be more feasible in L_2PbBr_4 in comparison to the L_2PbCl_4 or L_2PbI_4 to study their optical properties, which is discussed in the later section. L_2PbI_4 is green emitting in nature and has an optical absorption near 500 nm.

Mn(II) DOPING IN 2D-LAYERED PEROVSKITE

The mostly studied optical property of Mn(II) doping in 3D lead halide perovskite is $CsPbCl_3$, which has the ideal bandgap to transfer an efficient amount of excitonic energy to the Mn dopant state, to get a characteristic spin flipped emission of Mn dopant that originated from Mn d-d states $^4T_1$ to $^6A_1$ transition (Liu et al., 2016; Parobek et al., 2016; Guria et al., 2017; Mir et al., 2017; Dutta and Pradhan, 2019). L_2PbBr_4 is the alternative to the $CsPbCl_3$ because of their nearly identical bandgap differences. Similar to $CsPbCl_3$, the Mn(II)-doped L_2PbBr_4 has the excitonic emission near 400 nm, while highly intense Mn d-d emission near 600 nm. **Figure 2** presents a series of photoluminescence spectra, composed of different spacer ligands (L). The absorption and emission spectra of Mn^{2+}-doped (oleylammonium)$_2PbBr_4$ are presented in **Figures 2A,B**, respectively. The synthesis of

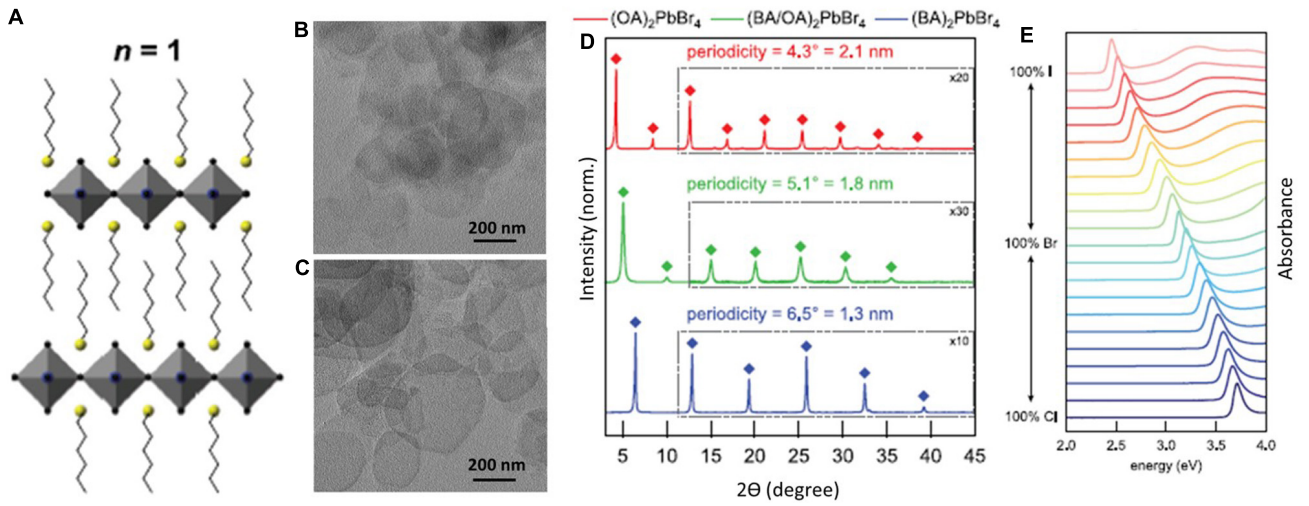

FIGURE 1 | (A) Schematic presentation of L_2PbX_4, where two successive corner-shared $[PbX_6]^{4-}$ are separated by two flipped organic ammonium ions. **(B,C)** TEM images of L_2PbCl_4 and L_2PbBr_4, respectively. **(D)** Powder x-ray diffraction patterns of $(OA)_2PbBr_4$ (red), $(OA/BA)_2PbBr_4$ (green), and $(BA)_2PbBr_4$ (blue) layered perovskites. Here, OA and BA stand for octylammonium and butylammonium, respectively. **(E)** Absorption spectra of L_2PbX_4 showing continuous tunability with the pure and mixed composition of halides. All figures are adapted from Weidman et al. (2016), with permission from the American Chemical Society.

this layered perovskite was carried out by mixing $PbBr_2$, $MnBr_2$, oleylamine, and oleic acid in 1-octadecene (ODE) in the presence of HBr. It was found that the presence of HBr played an important role for the formation of the layered perovskites, which helped dissolve the $MnBr_2$, and took part in the layered structures (Parobek et al., 2018). The highly emissive orange emission is known to be originated from the energy transfer of host exciton to dopant state. The inset of **Figure 2B** shows the illuminated digital image of a flask having the doped layered perovskites. The similar type of PL spectra originates when the spacer ligand is 1-napthylmethylammonium ion (NMA^+). Using these ligands, Mn(II)-doped $(NMA)_2PbBr_4$ film was prepared by spin coating the solution of (NMA)Br, $PbBr_2$, and $MnBr_2$ in DMF, previously annealed at 100°C for 2 h (Cortecchia et al., 2019). **Figure 2C** shows the PL spectra of undoped and 0.38% Mn(II)-doped butylammonium lead bromide single crystals. Herein, only 0.38% Mn(II) dopant incorporation leads to the highly intense dopant emission along with the minimized excitonic emission (Sheikh and Nag, 2019).

Figure 2D presents another set of Mn dopant concentration-dependent PL spectra of $(phenylethylammonium)_2PbBr_4$, where a minimum PL red shifting of approximately only 6 nm was observed with increasing the Mn dopant concentration in the layered structure. Here, the synthesis was carried out by mixing Pb(II)-acetate, Mn(II)-acetate, oleic acid, and phenylethylamine in ODE solvent. Then raising the temperature at 140°C, the required amount of trimethylsilyl bromide was injected, which acted as the bromide source. This doped layered perovskite that formed showed the highest PLQY (97%) of among the reported doped layered perovskite (Sun et al., 2019). The Mn dopant concentration was increased from 1 to 33%, and there was also a blue shift in the excitonic emission, and the Mn d-d emission that originates from the $^4T_1$-$^6A_1$ transition has a red shifting at the higher dopant concentration. The red shifting of Mn d-d emission due to the Mn–Mn interaction has a larger shift (approximately 25- to 40-nm red shift) is reported for Mn-doped $CsPbCl_3$ also (De et al., 2017; Das Adhikari et al., 2019a).

Mn(II) d-d EMISSION TUNABILITY

Apart from the PL red shifting, Mn concentration increment into the layered structure also enhanced the Mn d-d emission successively. **Figures 2E–H** present such kind of Mn concentration–dependent PL spectra with different spacer ligands that were used. **Figure 2E** presents the PL spectra of different percentages of Mn-substituted EA_2PbBr_4. This was prepared by following the ligand-assisted reprecipitation method, by dissolving ethylammonium bromide, $PbBr_2$ and different amounts of $MnBr_2$ in a polar solvent (DMF), followed by the addition of this dissolved precursor solution into the vigorously stirring toluene. Here, the quantum yield of Mn dopant emission was increased with increasing the Mn dopant concentrations, and the quantum yield obtained 78%, at the dopant level of 40% with respect to Pb (Luo et al., 2019). **Figures 2F–G** present Mn concentration–dependent PL spectra for the Mn-doped butylammonium lead bromide powder samples and single crystals, respectively, where the Mn d-d emission was increased with increasing the dopant concentration (Biswas et al., 2017; Dutta S. K. et al., 2019). Synthetic procedures of these products are discussed in later section Effect of thermal annealing of Mn(II)-doped 2D-Layered perovskite.

Figure 2H presents a set of PL spectra of undoped and doped $(C_6H_{18}N_2O_2)PbBr_4$ at different Mn concentrations. The synthesis was carried out by mixing $PbBr_2$ and $C_6H_{16}N_2O_2$ in HBr under vigorous stirring at 60°C and washed in

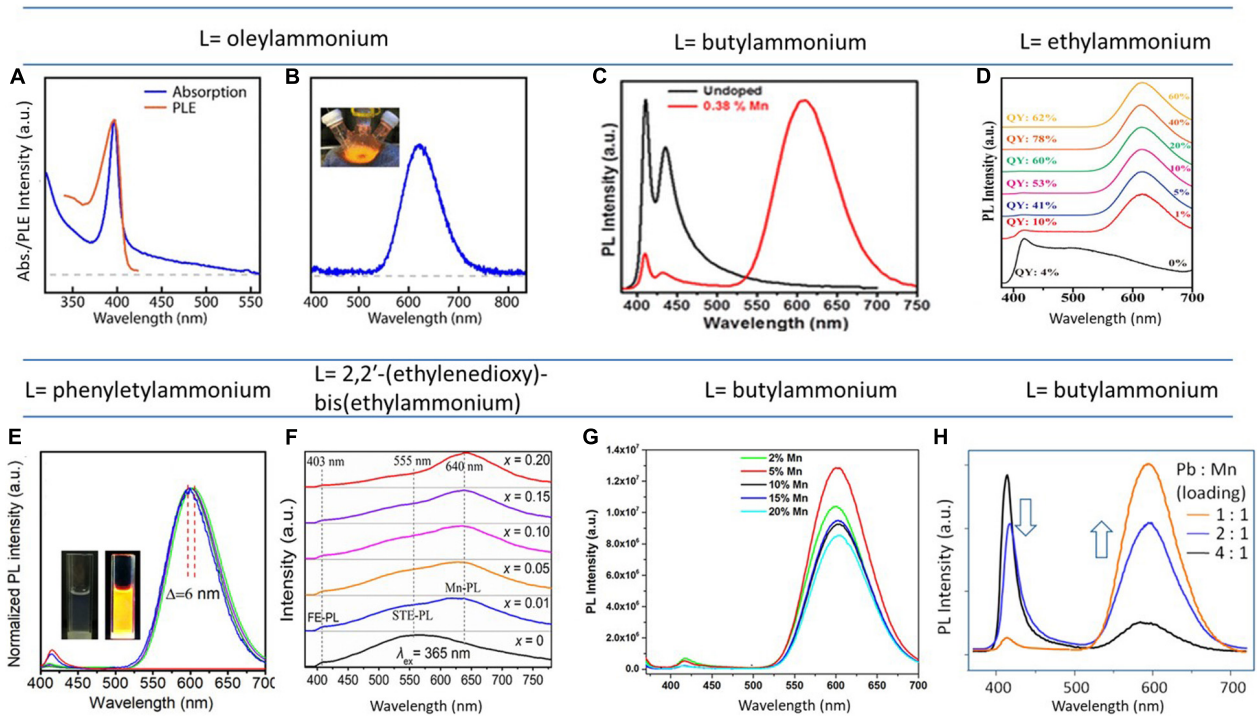

FIGURE 2 | (A) Absorbance, PLE, and **(B)** PL spectra of (oleylammonium)$_2$PbBr$_4$; inset is showing the illuminated three-necked flask having orange emission. **(C)** The PL spectra of undoped (black) and Mn(II)-doped (red) butylammonium lead bromide single crystals. Mn concentration–dependent PL spectra of Mn-doped L2PbBr$_4$, when the corresponding spacer ligand (L) is **(D)** phenylethylammonium, **(E)** ethylammonium, **(F,G)** butylammonium and **(H)** 2,2'-(ethylenedioxy)-bis(ethylammonium). **(A,B)** are adapted from Parobek et al. (2018), with permission from the American Chemical Society. **(C)** is adapted from Sheikh and Nag (2019), with permission from the American Chemical Society. **(D–H)** are reproduced from Biswas et al., 2017; Dutta S. K. et al., 2019; Luo et al., 2019; Sun et al., 2019; Zhou et al., 2019, with permission from the American Chemical Society.

ethanol. The supernatant was discarded, and the polycrystalline powder product was collected. For doping, different amounts of $MnBr_2{\cdot}5H_2O$ were taken along with $PbBr_2$. The undoped $(C_6H_{18}N_2O_2)PbBr_4$ has a broad emission at 403 and 555 nm (**Figure 2H**, bottom line spectrum) with the 365-nm excitation. The peak position at 403 nm is attributed to excitonic emission, and the broad peak position at 555 nm with a large Stokes shift is assigned as the self-trapped exciton (STE) emission due to the strong electron–lattice coupling at this deformable structure. When Mn was doped into this layered structure, an Mn dopant characteristic peak arises at 640 nm and produces highly intense white light emission due to covering the entire visible range. Similar to previous observations, the PL emission peak position at 640 nm was increased with increasing the dopant concentration (Zhou et al., 2019).

EFFECT OF THERMAL ANNEALING OF Mn(II)-DOPED 2D-LAYERED PEROVSKITE

Biswas et al. (2017) have followed the mechanochemical approach for the preparation of host BA_2PbBr_4, followed by the thermal annealing with $MnBr_2$ at the desired temperature for the preparation of Mn-doped BA_2PbBr_4. They have reported that the thermal annealing has an important role for controlling the incorporation of Mn dopants into the layered perovskite. The corresponding annealing temperature varied PL spectra are presented in **Figure 3A**. With increasing the annealing temperature starting from room temperature to 125°C, the Mn d-d emission intensity was found to be increased. When the sample is annealed at room temperature, there is a strong band-edge emission along with the weak Mn dopant emission. When the sample was annealed at 125°C, the band-edge emission is heavily suppressed and the dopant emission highly intensified. The main reason is only for increasing the thermal diffusion of dopant ions at a higher annealing temperature (here, 125°C).

Another report of our previous work on Mn-doped $(BA)_2PbBr_4$ microcrystals also predicts a similar effect on thermal annealing at 200°C (Dutta S. K. et al., 2019). This was synthesized by loading all precursors ($PbBr_2$, $MnBr_2$, butylammonium bromide, and HBr) in ODE and heated at 120°C. First, the as-prepared samples were drop-casted onto a glass slide; the structural and optical characterizations were carried out. After this, the same slide was heated at 200°C for 1 h in an inert atmosphere, followed by the structural and optical measurements that were carried out. The corresponding PL spectra of 1-h annealed samples and the as-prepared samples are presented in **Figure 3B**. The intensity of the excitonic and the dopant emission was more or less similar for the as-prepared sample, but the dopant emission was enhanced, and the excitonic emission was suppressed surprisingly after the thermal annealing

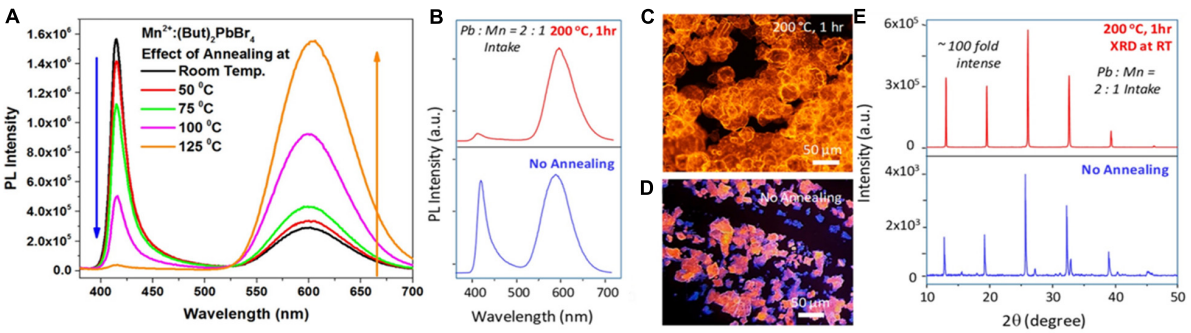

FIGURE 3 | (A) PL spectra of Mn^{2+}-doped (butylammonium)$_2PbBr_4$ annealed at different temperature. **(B)** PL spectra of Mn-doped (butylammonium)$_2PbBr_4$ microcrystals after (top, red) and before (bottom, blue) annealing at 200°C for 1 h, **(C,D)** optical microscopic images under UV irradiation (λ = 340-380 nm), and **(E)** corresponding powder XRD patterns. **(A,B–E)** are adapted from Biswas et al. (2017) and Dutta S. K. et al. (2019), respectively, with permission from the American Chemical Society.

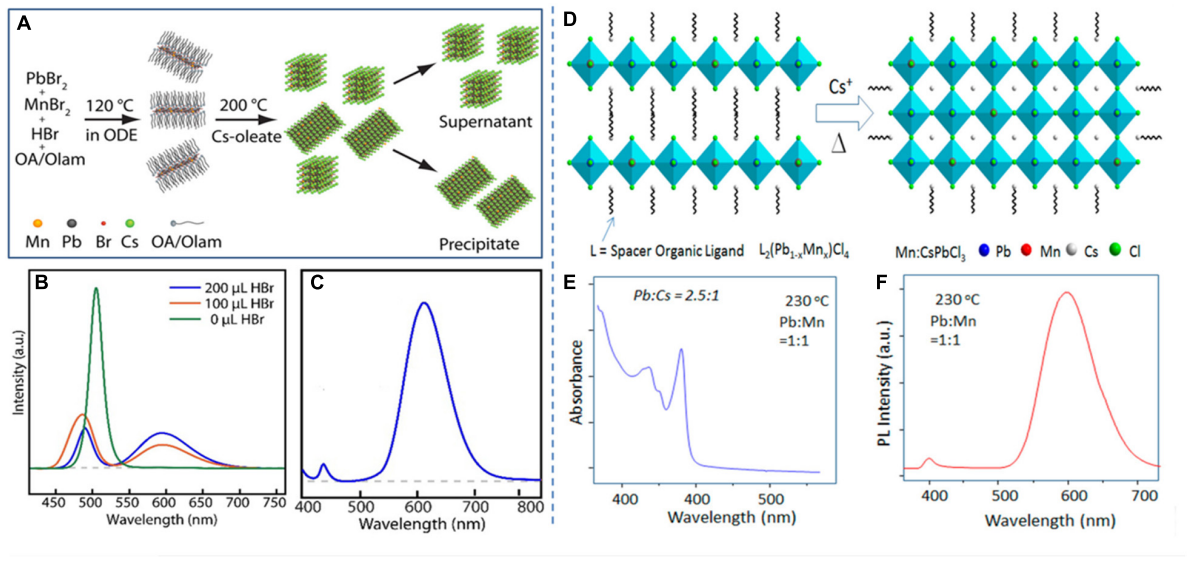

FIGURE 4 | (A) Schematic presentation of the stepwise formation of Mn-doped $CsPbBr_3$ nanocubes and nanoplatelets via the formation of Mn-doped L_2PbBr_4 at 120°C. The PL spectra of **(B)** Mn-doped $CsPbBr_3$ nanocubes, at different amounts of HBr used during the reaction, and **(C)** Mn-doped $CsPbBr_3$ nanoplatelets. **(D)** Schematic presentation of the formation of layered perovskite to Mn-doped $CsPbCl_3$ nanoplatelets upon the thermal treatment of layered perovskites with Cs^+ precursor. **(E)** Absorbance spectrum and **(F)** corresponding PL spectrum of Mn-doped $CsPbCl_3$ nanoplatelets. **(A–C)** adapted from Parobek et al. (2018) and **(D–F)** adapted from Das Adhikari et al. (2018), with permission from the American Chemical Society.

at 200°C for 1 h. The optical microscopic images under the UV irradiation (λ = 340-380 nm) of these samples after and before thermal treatment are presented in **Figures 3C,D**, which shows the bigger and smaller microcrystals for the thermally annealed and as-prepared samples, respectively. The smaller microcrystals are the mixture of blue- and orange-emitting in nature, which reflect the equal intensity ratio of excitonic and dopant emission in the PL spectra. When the samples were heated for 1 h at 200°C, the smaller blue- and orange-emitting microcrystals are merged and form the only orange-emitting bigger microcrystals, which reflect the minimized excitonic emission along with the enhanced Mn d-d emission at the PL spectrum. This observation strongly supports the solid-state ripening of microcrystals, where the smaller undoped microcrystals are merged, and forms the bigger doped microcrystals. The powder XRD patterns of 1-h annealed sample and the as-prepared samples are presented in **Figure 3E**, where the peak intensities corresponding to (n00) planes have the multifold enhancement (∼100 fold) for the 1-h annealed microcrystals due to the increased grain size of post-annealed microcrystals.

2D-LAYERED PEROVSKITE TO DOPED PEROVSKITE

In a report by Parobek et al. (2018), the Mn-doped oleylammonium lead bromide layered perovskites are used as the template for the synthesis of 3D Mn-doped $CsPbBr_3$ nanocubes

and nanoplatelets. In such typical case, the Mn-doped–layered lead bromide perovskites are first prepared, followed by the treatment with Cs precursor to prepare a mixture of Mn-doped $CsPbBr_3$ nanocubes and nanoplatelets. **Figure 4A** presents the schematic presentation of the stepwise preparation of layered perovskite followed by Mn^{2+}-doped $CsPbBr_3$ nanocubes and nanoplatelets. The supernatant of the product solution contains the smaller nanocubes, which has a mild Mn dopant emission and a strong excitonic emission presented in **Figure 4B**. There is a strong dependence of HBr used during the synthesis on the Mn dopant emission of Mn-doped $CsPbBr_3$ nanocubes, due to the dissolution of $MnBr_2$ during the synthesis, which helps in the incorporation of Mn dopant at the Pb site. The precipitate of the product solution contains the Mn-doped $CsPbBr_3$ platelets, which has the dominated Mn d-d emission, and the minimized excitonic emission arises from the nanoplatelets, which is presented in **Figure 4C**.

In one of our previous report, we have also used $L_2(Pb_{1-x}Mn_x)Cl_4$ layered perovskite, as the template for the preparation of Mn-doped $CsPbCl_3$ nanoplatelets, when these layered structures were thermally treated with Cs^+ precursor (Das Adhikari et al., 2018). The schematic presentation of such typical process is presented in **Figure 4D**. There was a fine control over the platelet dimension as a function of Mn^{2+} ions present into the layered structure. The platelet dimension was found to be decreased with increasing the Mn content into the layered structure. **Figure 4E** presents the sharp absorbance spectrum of Mn-doped $CsPbCl_3$ nanoplatelets, obtained by the thermal treatment of Cs-oleate with the highly Mn^{2+}-incorporated layered lead chloride perovskite. The sharp absorbance indicates the fine control of nanoplatelets size uniformity. The Mn-doped $CsPbCl_3$ nanoplatelets have dominated Mn d-d emission along with the negligible excitonic emission, which is presented in **Figure 4F**.

CONCLUSION AND FUTURE PROSPECTS

The advanced synthetic strategies for 2D-layered perovskites, Mn(II)-doped–layered perovskites, and the all-inorganic 2D platelet–shaped Mn(II)-doped $CsPbBr_3$ and $CsPbCl_3$ perovskite nanostructures are reported. The review discussed from the basic concepts of layered perovskites, their formation, Mn(II) doping, and appearance of Mn d-d emission and finally presented layered to doped 2D platelets of 3D perovskite nanostructures. It also covered all reports that appeared in and accepted by the community. Methodology and findings reported here are timely and would help the community for the future progress on developing more on the layered and 2D perovskites, and the future prospects for further development are as follows:

One pot generic synthesis could be implemented by the incorporation of different chain lengths of alkylammonium ions and to tune their respective bandgaps, by controlling the chain length of spacer cations, as well as the halide ions. Thermal annealing causes fusion of small single crystalline-layered perovskite to a comparative bigger structure. The application of such single crystalline-layered perovskite with large dimension would be more fantastic.

Unlike Mn(II)-doped $CsPbCl_3$, low-temperature optical properties of Mn(II)-doped L_2PbBr_4 are still elusive and need to be explored. The exciton to dopant energy transfer mechanism also needs to be explored, which is well understood for Mn(II)-doped $CsPbCl_3$.

Mn(II) doping in $CsPbI_3$ results enhanced stability. Thermal treatment of Cs(I) with Mn(II)-doped–layered lead iodide perovskite would prepare more stable Mn(II)-doped $CsPbI_3$ perovskites.

AUTHOR CONTRIBUTIONS

SD and NP designed the concept and wrote the manuscript. Both authors contributed to the article and approved the submitted version.

ACKNOWLEDGMENTS

DST of India is acknowledged for funding.

REFERENCES

Ba, Q., Jana, A., Wang, L., and Kim, K. S. (2019). Dual emission of water-stable 2D organic–inorganic halide perovskites with Mn(II) dopant. *Adv. Funct. Mater.* 29:1904768. doi: 10.1002/adfm.201904768

Bakthavatsalam, R., Biswas, A., Chakali, M., Bangal, P. R., Kore, B. P., and Kundu, J. (2019). Temperature-dependent photoluminescence and energy-transfer dynamics in Mn^{2+}-doped $(C_4H_9NH_3)_2PbBr_4$ two-dimensional (2D) layered perovskite. *J. Phys. Chem. C* 123, 4739–4748. doi: 10.1021/acs.jpcc.9b00207

Beck, H., Gehrmann, C., and Egger, D. A. (2019). Structure and binding in halide perovskites: analysis of static and dynamic effects from dispersion-corrected density functional theory. *APL Mater.* 7:021108. doi: 10.1063/1.5086541

Biswas, A., Bakthavatsalam, R., and Kundu, J. (2017). Efficient exciton to dopant energy transfer in Mn^{2+}-doped $(C_4H_9NH_3)_2PbBr_4$ two-dimensional (2D) layered perovskites. *Chem. Mater.* 29, 7816–7825. doi: 10.1021/acs.chemmater.7b02429

Blancon, J. C., Tsai, H., Nie, W., Stoumpos, C. C., Pedesseau, L., Katan, C., et al. (2017). Extremely efficient internal exciton dissociation through edge states in layered 2D perovskites. *Science* 355:1288. doi: 10.1126/science.aal4211

Chen, X., Lu, H., Yang, Y., and Beard, M. C. (2018). Excitonic effects in methylammonium lead halide perovskites. *J. Phys. Chem. Lett.* 9, 2595–2603. doi: 10.1021/acs.jpclett.8b00526

Cortecchia, D., Mróz, W., Neutzner, S., Borzda, T., Folpini, G., Brescia, R., et al. (2019). Defect engineering in 2D perovskite by Mn(II) doping for light-emitting applications. *Chem* 5, 2146–2158. doi: 10.1016/j.chempr.2019.05.018

Cortecchia, D., Neutzner, S., Srimath Kandada, A. R., Mosconi, E., Meggiolaro, D., De Angelis, F., et al. (2017). Broadband emission in two-dimensional hybrid perovskites: the role of structural deformation. *J. Am. Chem. Soc.* 139, 39–42. doi: 10.1021/jacs.6b10390

Das Adhikari, S., Behera, R. K., Bera, S., and Pradhan, N. (2019a). Presence of metal chloride for minimizing the halide deficiency and maximizing the doping efficiency in Mn(II)-doped $CsPbCl_3$ nanocrystals.". *J. Phys. Chem. Lett.* 10, 1530–1536. doi: 10.1021/acs.jpclett.9b00599

Das Adhikari, S., Dutta, A., Dutta, S. K., and Pradhan, N. (2018). Layered perovskites $L_2(Pb_{1-x}Mn_x)Cl_4$ to Mn-doped $CsPbCl_3$ perovskite platelets. *ACS Energy Lett.* 3, 1247–1253. doi: 10.1021/acsenergylett.8b00653

Das Adhikari, S., Guria, A. K., and Pradhan, N. (2019b). Insights of doping and the photoluminescence properties of Mn-doped perovskite nanocrystals. *J. Phys. Chem. Lett.* 10, 2250–2257. doi: 10.1021/acs.jpclett.9b00182

De, A., Mondal, N., and Samanta, A. (2017). Luminescence tuning and exciton dynamics of Mn-doped $CsPbCl_3$ nanocrystals. *Nanoscale* 9, 16722–16727.

Di Stasio, F., Christodoulou, S., Huo, N., and Konstantatos, G. (2017). Near-unity photoluminescence quantum yield in $CsPbBr_3$ nanocrystal solid-state films via postsynthesis treatment with lead bromide. *Chem. Mater.* 29, 7663–7667.

Dou, L., Wong, A. B., Yu, Y., Lai, M., Kornienko, N., Eaton, S. W., et al. (2015). Atomically thin two-dimensional organic-inorganic hybrid perovskites. *Science* 349:1518.

Dutta, A., Behera, R. K., Pal, P., Baitalik, S., and Pradhan, N. (2019). Near-unity photoluminescence quantum efficiency for all $CsPbX_3$ (X=Cl, Br, and I) perovskite nanocrystals: a generic synthesis approach. *Angew. Chem. Int. Ed.* 58, 5552–5556. doi: 10.1002/anie.201900374

Dutta, S. K., Dutta, A., Das Adhikari, S., and Pradhan, N. (2019). Doping Mn^{2+} in single-crystalline layered perovskite microcrystals. *ACS Energy Lett.* 4, 343–351. doi: 10.1021/acsenergylett.8b02349

Dutta, S. K., and Pradhan, N. (2019). Coupled halide-deficient and halide-rich reaction system for doping in perovskite armed nanostructures. *J. Phys. Chem. Lett.* 10, 6788–6793. doi: 10.1021/acs.jpclett.9b02860

Even, J., Pedesseau, L., and Katan, C. (2014). Understanding quantum confinement of charge carriers in layered 2D hybrid perovskites. *Chem. Phys. Chem.* 15, 3733–3741. doi: 10.1002/cphc.201402428

Guria, A. K., Dutta, S. K., Das Adhikari, S., and Pradhan, N. (2017). Doping Mn^{2+} in lead halide perovskite nanocrystals: successes and challenges. *ACS Energy Lett.* 2, 1014–1021. doi: 10.1021/acsenergylett.7b00177

Jena, A. K., Kulkarni, A., and Miyasaka, T. (2019). Halide perovskite photovoltaics: background, status, and future prospects. *Chem. Rev.* 119, 3036–3103. doi: 10.1021/acs.chemrev.8b00539

Kanwat, A., Moyen, E., Cho, S., and Jang, J. (2018). Rubidium as an alternative cation for efficient perovskite light-emitting diodes. *ACS Appl. Mater. Interfaces* 10, 16852–16860. doi: 10.1021/acsami.8b01292

Kato, M., Suzuki, A., Ohishi, Y., Tanaka, H., and Oku, T. (2018). Fabrication and characterization of rubidium/formamidinium-incorporated methylammonium-lead-halide perovskite solar cells. *AIP Conf. Proc.* 1929:020015.

Kim, H., Lim, K.-G., and Lee, T.-W. (2016). Planar heterojunction organometal halide perovskite solar cells: roles of interfacial layers. *Energy Environ. Sci.* 9, 12–30. doi: 10.1039/c5ee02194d

Kojima, A., Teshima, K., Shirai, Y., and Miyasaka, T. (2009). Organometal halide perovskites as visible-light sensitizers for photovoltaic cells. *J. Am. Chem. Soc.* 131, 6050–6051. doi: 10.1021/ja809598r

Koutselas, I., Bampoulis, P., Maratou, E., Evagelinou, T., Pagona, G., and Papavassiliou, G. C. (2011). Some unconventional organic-inorganic hybrid low-dimensional semiconductors and related light-emitting devices. *J. Phys. Chem. C* 115, 8475–8483. doi: 10.1021/jp111881b

Kovalenko, M. V., Protesescu, L., and Bodnarchuk, M. I. (2017). Properties and potential optoelectronic applications of lead halide perovskite nanocrystals. *Science* 358:745. doi: 10.1126/science.aam7093

Kumar, S., Jagielski, J., Yakunin, S., Rice, P., Chiu, Y.-C., Wang, M., et al. (2016). Efficient blue electroluminescence using quantum-confined two-dimensional perovskites. *ACS Nano* 10, 9720–9729. doi: 10.1021/acsnano.6b05775

Lan, C., Zhou, Z., Wei, R., and Ho, J. C. (2019). Two-dimensional perovskite materials: from synthesis to energy-related applications. *Mater. Today Energy* 11, 61–82. doi: 10.1016/j.mtener.2018.10.008

Leijtens, T., Bush, K., Cheacharoen, R., Beal, R., Bowring, A., and McGehee, M. D. (2017). Towards enabling stable lead halide perovskite solar cells; interplay between structural, environmental, and thermal stability. *J. Mater. Chem. A* 5, 11483–11500.

Lermer, C., Senocrate, A., Moudrakovski, I., Seewald, T., Hatz, A.-K., Mayer, P., et al. (2018). Completing the picture of 2-(aminomethylpyridinium) lead hybrid perovskites: insights into structure, conductivity behavior, and optical properties. *Chem. Mater.* 30, 6289–6297. doi: 10.1021/acs.chemmater.8b01840

Li, J., Yu, Q., He, Y., Stoumpos, C. C., Niu, G., Trimarchi, G. G., et al. (2018). $Cs_2PbI_2Cl_2$, All-inorganic two-dimensional Ruddlesden–Popper mixed halide perovskite with optoelectronic response. *J. Am. Chem. Soc.* 140, 11085–11090. doi: 10.1021/jacs.8b06046

Li, Y., and Yang, K. (2019). High-throughput computational design of organic–inorganic hybrid halide semiconductors beyond perovskites for optoelectronics. *Energy Environ. Sci.* 12, 2233–2243. doi: 10.1039/c9ee01371g

Liang, D., Peng, Y., Fu, Y., Shearer, M. J., Zhang, J., Zhai, J., et al. (2016). Color-pure violet-light-emitting diodes based on layered lead halide perovskite nanoplates. *ACS Nano* 10, 6897–6904. doi: 10.1021/acsnano.6b02683

Liu, W., Lin, Q., Li, H., Wu, K., Robel, I., Pietryga, J. M., et al. (2016). Mn^{2+}-Doped lead halide perovskite nanocrystals with dual-color emission controlled by halide content. *J. Am. Chem. Soc.* 138, 14954–14961. doi: 10.1021/jacs.6b08085

Luo, B., Guo, Y., Li, X., Xiao, Y., Huang, X., and Zhang, J. Z. (2019). Efficient trap-mediated Mn^{2+} dopant emission in two dimensional single-layered perovskite $(CH_3CH_2NH_3)_2PbBr_4$. *J. Phys. Chem. C* 123, 14239–14245. doi: 10.1021/acs.jpcc.9b02649

Mao, L., Tsai, H., Nie, W., Ma, L., Im, J., Stoumpos, C. C., et al. (2016). Role of organic counterion in lead- and tin-based two-dimensional semiconducting iodide perovskites and application in planar solar cells. *Chem. Mater.* 28, 7781–7792. doi: 10.1021/acs.chemmater.6b03054

Mauck, C. M., and Tisdale, W. A. (2019). Excitons in 2D organic-inorganic halide perovskites. *Trends Chem.* 1, 380–393. doi: 10.1016/j.trechm.2019.04.003

Mir, W. J., Jagadeeswararao, M., Das, S., and Nag, A. (2017). Colloidal Mn-doped cesium lead halide perovskite nanoplatelets. *ACS Energy Lett.* 2, 537–543. doi: 10.1021/acsenergylett.6b00741

Mondal, N., De, A., and Samanta, A. (2019). Achieving near-unity photoluminescence efficiency for blue-violet-emitting perovskite nanocrystals. *ACS Energy Lett.* 4, 32–39. doi: 10.1021/acsenergylett.8b01909

Nedelcu, G., Protesescu, L., Yakunin, S., Bodnarchuk, M. I., Grotevent, M. J., and Kovalenko, M. V. (2015). Fast anion-exchange in highly luminescent nanocrystals of cesium lead halide perovskites ($CsPbX_3$, X = Cl, Br, I). *Nano Lett.* 15, 5635–5640. doi: 10.1021/acs.nanolett.5b02404

Park, S., Cho, H., Choi, W., Zou, H., and Jeon, D. Y. (2019). Correlation of near-unity quantum yields with photogenerated excitons in X-type ligand passivated $CsPbBr_3$ perovskite quantum dots. *Nanoscale Adv.* 1, 2828–2834. doi: 10.1039/c9na00292h

Parobek, D., Dong, Y., Qiao, T., and Son, D. H. (2018). Direct hot-injection synthesis of Mn-doped $CsPbBr_3$ nanocrystals. *Chem. Mater.* 30, 2939–2944. doi: 10.1021/acs.chemmater.8b00310

Parobek, D., Roman, B. J., Dong, Y., Jin, H., Lee, E., Sheldon, M., et al. (2016). Exciton-to-dopant energy transfer in Mn-doped cesium lead halide perovskite nanocrystals. *Nano Lett.* 16, 7376–7380. doi: 10.1021/acs.nanolett.6b02772

Pedesseau, L., Sapori, D., Traore, B., Robles, R., Fang, H.-H., Loi, M. A., et al. (2016). Advances and promises of layered halide hybrid perovskite semiconductors. *ACS Nano* 10, 9776–9786. doi: 10.1021/acsnano.6b05944

Protesescu, L., Yakunin, S., Bodnarchuk, M. I., Bertolotti, F., Masciocchi, N., Guagliardi, A., et al. (2016). Monodisperse formamidinium lead bromide nanocrystals with bright and stable green photoluminescence. *J. Am. Chem. Soc.* 138, 14202–14205. doi: 10.1021/jacs.6b08900

Protesescu, L., Yakunin, S., Bodnarchuk, M. I., Krieg, F., Caputo, R., Hendon, C. H., et al. (2015). Nanocrystals of cesium lead halide perovskites ($CsPbX_3$, X = Cl, Br, and I): novel optoelectronic materials showing bright emission with wide color gamut. *Nano Lett.* 15, 3692–3696. doi: 10.1021/nl5048779

Protesescu, L., Yakunin, S., Kumar, S., Bar, J., Bertolotti, F., Masciocchi, N., et al. (2017). Dismantling the "red wall" of colloidal perovskites: highly luminescent formamidinium and formamidinium-cesium lead iodide nanocrystals. *ACS Nano* 11, 3119–3134. doi: 10.1021/acsnano.7b00116

Sheikh, T., and Nag, A. (2019). Mn doping in centimeter-sized layered 2D butylammonium lead bromide (BA_2PbBr_4) single crystals and their optical properties. *J. Phys. Chem. C* 123, 9420–9427. doi: 10.1021/acs.jpcc.9b01550

Sheikh, T., Shinde, A., Mahamuni, S., and Nag, A. (2018). Possible dual bandgap in $(C_4H_9NH_3)_2PbI_4$ 2D layered perovskite: single-crystal and exfoliated few-layer. *ACS Energy Lett.* 3, 2940–2946. doi: 10.1021/acsenergylett.8b01799

Sichert, J. A., Hemmerling, A., Cardenas-Daw, C., Urban, A. S., and Feldmann, J. (2019). Tuning the optical bandgap in layered hybrid perovskites through variation of alkyl chain length. *APL Mater.* 7:041116. doi: 10.1063/1.5087296

Smith, I. C., Hoke, E. T., Solis-Ibarra, D., McGehee, M. D., and Karunadasa, H. I. (2014). A layered hybrid perovskite solar-cell absorber with enhanced moisture stability. *Angew. Chem.* 126, 11414–11417. doi: 10.1002/ange.201406466

Smith, I. C., Smith, M. D., Jaffe, A., Lin, Y., and Karunadasa, H. I. (2017). Between the sheets: postsynthetic transformations in hybrid perovskites. *Chem. Mater.* 29, 1868–1884. doi: 10.1021/acs.chemmater.6b05395

Smith, M. D., Connor, B. A., and Karunadasa, H. I. (2019). Tuning the luminescence of layered halide perovskites. *Chem. Rev.* 119, 3104–3139. doi: 10.1021/acs.chemrev.8b00477

Snaith, H. J. (2013). Perovskites: the emergence of a new era for low-cost, high-efficiency solar cells. *J. Phys. Chem. Lett.* 4, 3623–3630. doi: 10.1021/jz4020162

Soe, C. M. M., Nagabhushana, G. P., Shivaramaiah, R., Tsai, H., Nie, W., Blancon, J.-C., et al. (2019). Structural and thermodynamic limits of layer thickness in 2D halide perovskites. *Proc. Natl. Acad. Sci. U.S.A.* 116, 58–66. doi: 10.1073/pnas.1811006115

Stoumpos, C. C., Cao, D. H., Clark, D. J., Young, J., Rondinelli, J. M., Jang, J. I., et al. (2016a). Ruddlesden–Popper hybrid lead iodide perovskite 2D homologous semiconductors. *Chem. Mater.* 28, 2852–2867. doi: 10.1021/acs.chemmater.6b00847

Stoumpos, C. C., Soe, C. M. M., Tsai, H., Nie, W., Blancon, J.-C., Cao, D. H., et al. (2016b). High members of the 2D ruddlesden-popper halide perovskites: synthesis, optical properties, and solar cells of $(CH_3(CH_2)_3NH_3)_2(CH_3NH_3)_4Pb_5I_{16}$. *Chemistry* 2, 427–440. doi: 10.1016/j.chempr.2017.02.004

Sun, C., Gao, Z., Deng, Y., Liu, H., Wang, L., Su, S., et al. (2019). Orange to red, emission-tunable Mn-doped two-dimensional perovskites with high luminescence and stability. *ACS Appl. Mater. Interfaces* 11, 34109–34116. doi: 10.1021/acsami.9b11665

Tsai, H., Nie, W., Blancon, J.-C., Stoumpos, C. C., Asadpour, R., Harutyunyan, B., et al. (2016). High-efficiency two-dimensional Ruddlesden–Popper perovskite solar cells. *Nature* 536:312.

Vassilakopoulou, A., Papadatos, D., and Koutselas, I. (2016). Room temperature light emitting diode based on 2D hybrid organic-inorganic low dimensional perovskite semiconductor. *Appl. Mater. Today* 5, 128–133. doi: 10.1016/j.apmt.2016.09.004

Weidman, M. C., Seitz, M., Stranks, S. D., and Tisdale, W. A. (2016). Highly tunable colloidal perovskite nanoplatelets through variable cation, metal, and halide composition. *ACS Nano* 10, 7830–7839. doi: 10.1021/acsnano.6b03496

Yin, J., Maity, P., Xu, L., El-Zohry, A. M., Li, H., Bakr, O. M., et al. (2018). Layer-dependent Rashba band splitting in 2D hybrid perovskites. *Chem. Mater.* 30, 8538–8545. doi: 10.1021/acs.chemmater.8b03436

Yong, Z.-J., Guo, S.-Q., Ma, J.-P., Zhang, J.-Y., Li, Z.-Y., Chen, Y.-M., et al. (2018). Doping-enhanced short-range order of perovskite nanocrystals for near-unity violet luminescence quantum yield. *J. Am. Chem. Soc.* 140, 9942–9951. doi: 10.1021/jacs.8b04763

Yuan, M., Quan, L. N., Comin, R., Walters, G., Sabatini, R., Voznyy, O., et al. (2016). Perovskite energy funnels for efficient light-emitting diodes. *Nat. Nanotechnol.* 11:872.

Zhang, X., Li, L., Sun, Z., and Luo, J. (2019). Rational chemical doping of metal halide perovskites. *Chem. Soc. Rev.* 48, 517–539. doi: 10.1039/c8cs00563j

Zhou, G., Jiang, X., Molokeev, M., Lin, Z., Zhao, J., Wang, J., et al. (2019). Optically modulated ultra-broad-band warm white emission in Mn^{2+}-doped $(C_6H_{18}N_2O_2)PbBr_4$ hybrid metal halide phosphor. *Chem. Mater.* 31, 5788–5795. doi: 10.1021/acs.chemmater.9b01864

Conflict of Interest: The authors declare that the research was conducted in the absence of any commercial or financial relationships that could be construed as a potential conflict of interest.

Copyright © 2020 Das Adhikari and Pradhan. This is an open-access article distributed under the terms of the Creative Commons Attribution License (CC BY). The use, distribution or reproduction in other forums is permitted, provided the original author(s) and the copyright owner(s) are credited and that the original publication in this journal is cited, in accordance with accepted academic practice. No use, distribution or reproduction is permitted which does not comply with these terms.